Desalination and Water Treatment
www.deswater.com
doi: 10.5004/dwt.2019.23686

144 (2019) 79–88
March

Low-cost and efficient removal of mercury from contaminated water by novel nanoparticles from water industry waste

Elsayed Elkhatib[a,*], Mohamed Moharem[b], Hala Hamadeen[a]

[a]*Department of Soil and Water Sciences, Alexandria University, Alexandria 21545, Egypt, Tel./Fax: +002/03 5904684; emails: selkhatib1@yahoo.com (E. Elkhatib), halamahmoud119@hotmail.com (H. Hamadeen)*
[b]*Regional center for Food and Feed, Agricultural Research Center, Alexandria, Egypt, email: mlmoharem@hotmail.com*

Received 13 August 2018; Accepted 25 December 2018

ABSTRACT

Nanomaterials are efficient pollutant adsorbents due to their large specific surface area and multiple active sites. In the present research, the novel water treatment residual nanoparticles (nWTR) produced by precision milling were evaluated for their potential in removing Hg(II) from contaminated water. The operational parameters, stability of Hg sorbed onto nWTR, Hg desorption, and nWTR reusability were also investigated. The nWTR demonstrated high adsorption potential for Hg(II) with a removal efficiency of 93% within 15 min. Langmuir and Temkin isotherm models successfully described the sorption equilibrium while power function model best described Hg(II) sorption kinetics data. Fourier transform infrared spectroscopy analysis suggests that the hydroxyls may act as the surface active sites for Hg(II) binding to nWTR surfaces. The Hg(II) adsorption by nWTR declined as the pH increased from 3 to 11 as a result of increasing OH^- ligand concentration with increasing pH. The low percentage (0.11%) of Hg(II) released from Hg-loaded nWTR after four consecutive desorption cycles and the association of high percentage (80%) of sorbed Hg with the residual fraction ascertained immobilization and high stability of Hg sorbed by nWTR. Application study confirmed the potential and efficiency of nWTR to remediate Hg(II) polluted wastewater.

Keywords: Adsorption; Desorption; Kinetic models; Fractionation; Wastewater

1. Introduction

Aquatic ecosystem contamination especially with heavy metal ions is causing serious environmental and health problems worldwide. Of all contaminant metals, mercury is classified as one of the most toxic heavy metals since it is nonbiodegradable and causes human deaths through the ingestion of contaminated aquatic organisms [1,2]. The mercury pollution arises mainly from the industries involved in mining, dry cell batteries, fluorescent light bulbs, switches, cement, metal plating, seed dressings, fungicides, and paints [3,4].

Many technologies are recently available to use for remediation of Hg-contaminated water [3,5]. However, most of these technologies have shown limitations in removing the toxic contaminants from contaminated water to safe levels as well as they are costly, laborious, and time consuming [6,7]. Thus, developing inexpensive efficient yet green remediation techniques remains a challenge.

The low-cost and eco-friendly water treatment residuals (WTRs) and water industry waste have become popular recently because of their amorphous nature and high sorption affinity toward heavy metals [8–10]. Conclusive prior studies have shown that WTR particles in microscale greatly increase their active surface areas and consequently their adsorption capacity for heavy metals [11]. Recently, Elkhatib et al. [12] produced nanoparticle sorbents (WTR nanoparticles (nWTRs) < 100 nm) from water treatment residues using milling. The *P* sorption capacity of nWTR

* Corresponding author.

produced has been reported to be 30 times higher than that of bulk WTR [12]. The comparatively greater adsorption capability of nWTR suggests its promising applicability toward remediation of various environmental contaminants [13].

The potential use of bulk WTRs, inexpensive and nonhazardous waste material, for the removal of heavy metals is evident [14]. However, data are not available in the literature on the use of nanoscale WTR as super adsorbent for mercury (II) removal. Here we report a comparative study of bulk WTRs and nWTR for treatment of Hg(II)-contaminated water. The objectives of this study were therefore (i) to determine mercury adsorption capacity of nWTRs and to investigate the pertinent adsorption mechanism and (ii) to study the effects of operational parameters including adsorbent dosage, solution pH, and coexisting cations on the removal of Hg by nWTRs.

2. Materials and methods

2.1. Synthesis and characterization of nWTR

The bulk WTR (mWTR) was collected from Kafr El-Dawar water treatment plant in El-bohera, Egypt. The mWTR samples were air dried, ground, and passed through two different sieves having 2 mm and 51 μm pore diameters. Fritsch planetary mono mill was used to produce nanoscale WTR (nWTR) following the method of Elkhatib et al. [12]. Transmission electron microscopy, X-ray diffraction, and scanning electron microscopy (SEM) with energy-dispersive X-ray (EDX) (INCAx-Sight model 6587, Oxford Instruments, UK) were used to characterize and determine elemental contents of nWTR, mWTR, and uWTR. Surface area analyzer (Quantachrome, USA) was used for specific surface area (SSA) determination [15].

2.2. Sorption isotherms and maximum sorption capacity of nWTRs

The maximum sorption capacity of three sizes of WTRs for Hg(II) was determined in batch adsorption experiments. The three sizes of WTR used in the adsorption study were mWTR (<2 mm), uWTR (<51 μm), and nWTR (<100 nm). Solutions with final Hg^{2+} concentrations of 5, 10, 20, 40, 80, and 160 mg L^{-1} were prepared using $Hg(NO_3)_2$ standard solution obtained from Fisher Scientific , Leicestershire, England. Solutions obtained were placed in contact with WTR materials in 50 mL capped polypropylene tubes, equilibrated on an end-over-end shaker (4 rpm) for 24 h, centrifuged at 4,000 rpm for 10 min, and filtered through a 0.45 μm Millipore filter. All experiments were run-in triplicate at pH 7.2, and the filtered solutions were analyzed for total Hg concentration by inductively coupled plasma spectrometry (ICPS). The sorption data were then fit to different isotherm models, and the maximum sorption capacity was calculated using the best fit model. The SEM-EDX instruments were used to examine and determine Hg sorbed by nWTR.

To study the influence of nWTR dosage on the Hg removal, three nWTR masses (0.02, 0.05, and 0.10 g) were shaken with 10 mL each of different Hg concentrations (0–500 mg L^{-1}) contained in 50 mL centrifuge tubes for 24 h using end-over-end shaker. The suspensions were then centrifuged at 4,000 rpm for 10 min, and the supernatant solutions were filtered through a 0.45 μm membrane filter (Millipore), and the residual (RS) Hg concentrations were determined using ICPS.

2.3. Effect of initial concentration and co-ions

The effect of extent of adsorption by different initial Hg concentrations (5, 20, 40, 80, and 160 mg L^{-1}) was investigated. The experiments were carried out by adding 0.10 g of nWTR sample into 20 mL of Hg solutions, and the mixtures were shaken for 24 h using end-over-end shaker. After centrifugation, the solutions were transferred into clean tubes and refrigerated (−4°C) until analysis. To study the influence of coexisting ions on Hg adsorption by nWTR, similar set of experiments were run in the presence of two competing cations (As and Cr) at concentrations equal to Hg concentration.

2.4. Adsorption kinetics

Adsorption kinetic experiments were performed at room temperature (23°C) using the batch technique. A dose of nWTR (100 mg) and 20 mL of Hg solutions with the initial concentration of 350 mg L^{-1} were put in 50 mL centrifuge tubes and shaken using an end-over-end shaker for different time intervals at 3 different pH levels (pH 5, 7, and 9). The pH of each suspension was adjusted by adding 0.1 HCl or 0.1 NaOH using the automatic titrator. The Hg-nWTR suspensions were centrifuged at 4,000 rpm for 10 min, and the solutions were filtered through a 0.45 μm Millipore filter. The Hg concentrations in the filtrate were analyzed using ICPS. The kinetics of Hg adsorption on the nWTR samples was investigated by fitting the sorption data to power function, parabolic diffusion, first-order, and Elovich kinetic models.

3. Results and discussion

3.1. Surface characteristics and chemical composition of mWTR, uWTR, and nWTR

The microstructure of mWTR and uWTR particles as examined by SEM suggests amorphous irregular shapes with 'rough' surface and the presence of micropores [12]. SEM-EDX elemental analysis revealed that Si, Al, and Fe in mWTR and uWTR represent around 77% of the total elements. After milling, the Si and Al contents of the feed uWTR decreased from 43.77% to 21.20% and from 16.4% to 6.33%, respectively, while total iron increased substantially from 15.63% to 43.97%. The nWTR particles are largely spherical in the 45–96 nm size range (Fig. 1(a)). The scanning images of nWTR surface before and after Hg sorption (Figs. 1(a) and (b)) show a coating layer of adsorbed Hg on nWTR surface after Hg addition. The spectra of SEM–EDX analysis have shown an emerging Hg peak (4.90%) that represents the Hg ions adsorbed by nWTR and a clear reduction in the intensity of the Ca and Si peaks (Fig. 1(b)).

3.2. Specific surface area

The classic Brauner–Emmette–Teller technique [15] was used for SSA and total pore volume (TPV) determination

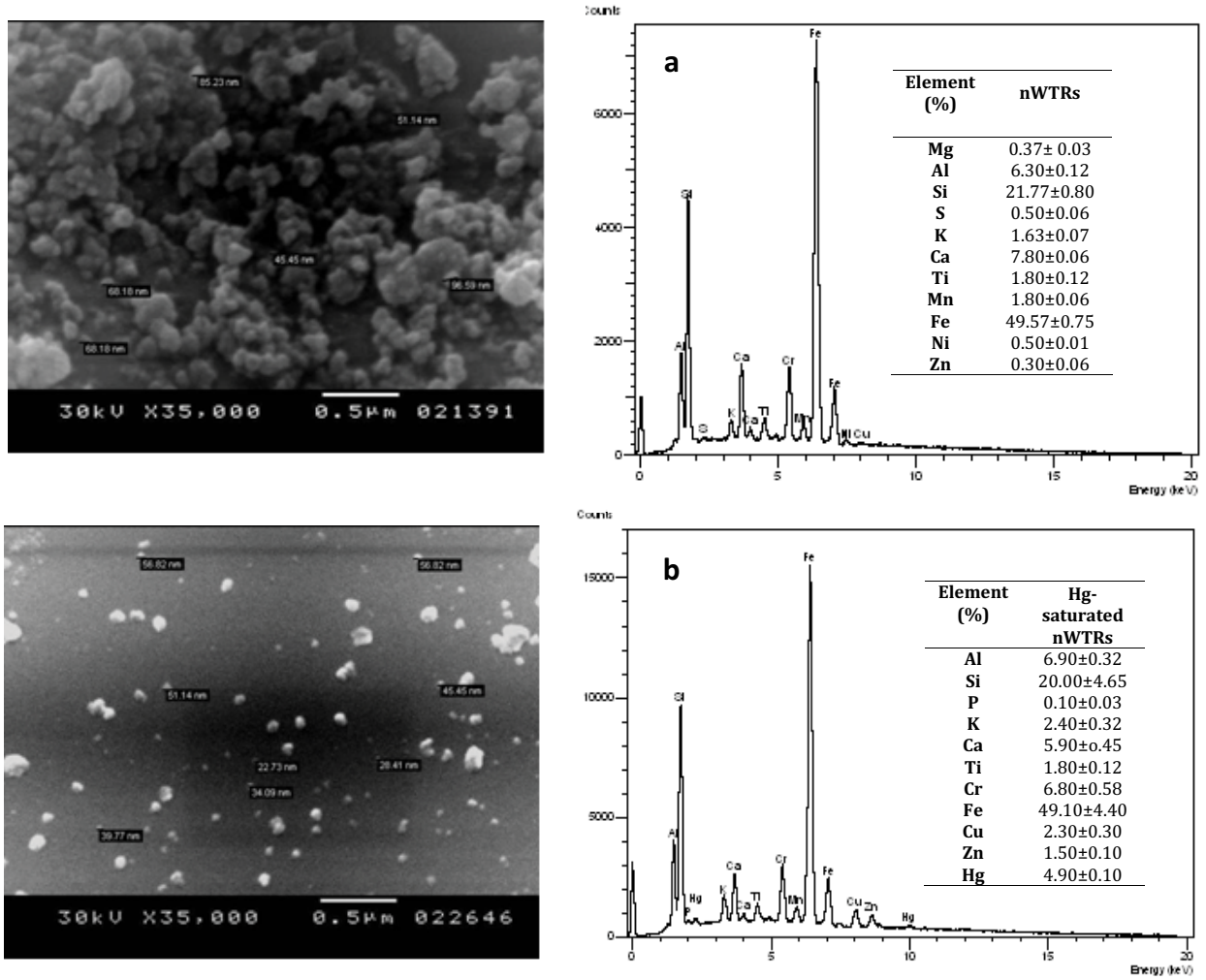

Fig. 1. Scanning electron microscopy (SEM) image and energy-dispersive X-ray (EDX) spectrum of (a) nWTR and (b) Hg-saturated nWTR.

of mWTR, uWTR, and nWTR samples. The mWTR has an SSA of 53.1 $m^2 g^{-1}$ and has TPV of 0.020 $cm^3 g^{-1}$ while uWTR has SSA of 66.5 $m^2 g^{-1}$ and TPV of 0.025 $cm^3 g^{-1}$. After 75 min of milling, SSA and TPV of uWTR increased to 129.0 $m^2 g^{-1}$ and 0.051 $cm^3 g^{-1}$, respectively. The SSA of nWTR sample is 2–3 times higher than that of mWTR, and therefore, a large enhancement of its reactivity is anticipated. Because SSA strongly influences solid surface reactivity [16], a large SSA makes nanostructure materials ideal candidates for water treatment and desalination.

3.3. Fourier transmission infrared spectroscopy

The differences in the chemical features of nWTR before and after Hg adsorption are shown in Fourier transmission infrared (FTIR) spectra (Fig. 2). Before Hg adsorption, the bands at 3,416 and 1,636 cm^{-1} in the FTIR spectrum of nWTR are assigned to the HO–H stretching and bending vibrations, respectively [16]. After Hg adsorption, the three small peaks located between 3,713 and 4,012 cm^{-1} (attributed to the dangling O–H bonds on the surface of the H_2O layer in nWTR) shifted to different frequencies (Fig. 2). However, due to the fact that stronger bonds usually vibrate faster than weaker bonds [17], the bands at 3,416 and 1,636 cm^{-1} were greatly increased in the intensity and shifted to lower wave numbers 3,410 and 1,635 cm^{-1}, respectively. The shift of aforementioned peaks and bands demonstrated the involvement of OH groups of nWTRs in the retention of Hg. After Hg adsorption, shifts in the peaks at 1,448 and 1,091 cm^{-1} on the surface of WTR before Hg sorption to wave numbers 1,459 and 1,039 cm^{-1} were also noticed suggesting molecular interactions between Hg and nWTR [18,19]. In addition, the shift of the peaks at 1,091 and 543 cm^{-1} (O–Al–O stretching vibrations) on the surface of nWTR to lower wave numbers 1,039 and 539 cm^{-1}, respectively, after Hg adsorption clearly pinpoints the interaction of O–Al–O of nWTR with Hg^{2+} ions [20].

3.4. Fractionation of the Hg-saturated nWTR and Hg mobility

To evaluate the potential mobility of Hg sorbed onto nWTR relative to mWTR and uWTR, the mercury (Hg) distribution in the fractions of the sorbents was performed

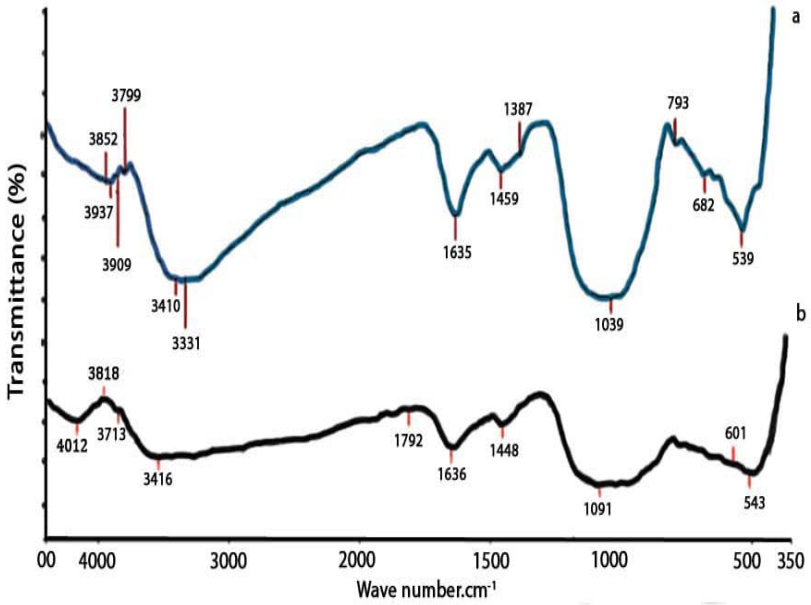

Fig. 2. Infrared spectra. (a) Hg-saturated nWTRs and (b) nonsaturated nWTRs.

on the Hg-saturated sorbent (nWTR) using the fractionation scheme of Tessier et al. [21]. The sequential extractions have been commonly used for Hg speciation because of the efficiency and reproducibility of the procedure [22]. According to the scheme, the labile Hg associated with the RS fraction is less mobile than Hg associated with the nonresidual (NORS) fraction (sum of all fractions except the RS fraction). Such an approach enables us to correlate the Hg data with sorbent fractions and identify the mobility of Hg bound to different sorbent fractions. The Hg fractionation results (Fig. 3) show that Hg adsorbed on mWTR was mostly associated with the more mobile NORS fraction (59%), whereas 80% of Hg on nWTR was associated with the RS fraction, the less mobile fraction. Such differences could be related to particle size and crystalline effects, which in turn affect the solubility of Hg phases present [22]. This finding is in agreement with the result obtained by Quinones et al. [23] who found an increase of Hg in WTR fraction over time, as they referred this observation to increase initially amorphous mineral crystallinity degree suggesting that during aging Hg loaded into WTR could become part of the RS fraction. A greater percentage of Hg associated with the RS fraction of nWTR relative to mWTR and uWTR indicates the higher capability of nWTR to immobilize Hg than bulk WTR (mWTR). These observations support the hypothesis that the smaller size and the higher surface area of WTR nanoparticles greatly enhance its sorptive characteristics and stability.

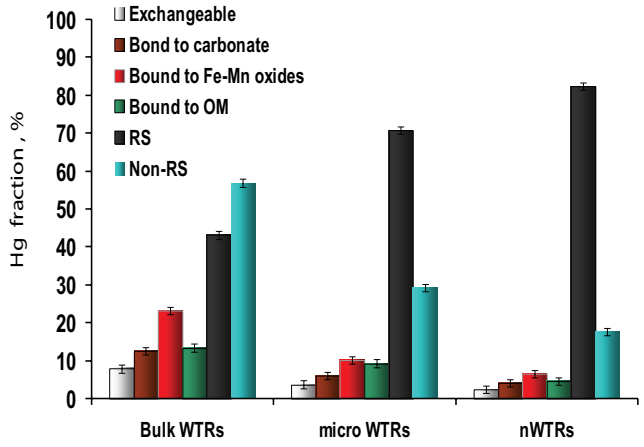

Fig. 3. Fractionation of adsorbed Hg(II) on different particle sizes of WTR. Notice that Hg adsorbed on nWTR was mostly associated with the less mobile fraction (residual fraction, RS), which indicates the high capability of nWTR to immobilize Hg(II).

3.5. Adsorbent dose

The effect of nWTR dose (0.020–0.10 g L^{-1}) on the adsorption of Hg was tested, and the results are shown in Fig. 4. The amount of sorbed Hg was more pronounced at high dose of nWTR and showed an H-type isotherm according to Giles isotherm classification [24]. This type of isotherm indicates a strong affinity between Hg and

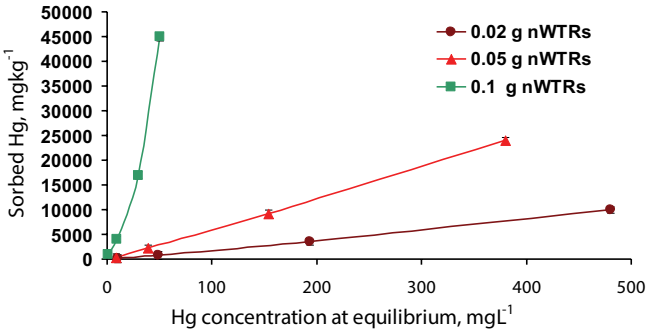

Fig. 4. Effect of adsorbent dose on Hg sorbed by nWTR. Adsorption of Hg increases rapidly with increasing adsorbent dose of nWTR from 0.020 to 0.10 g.

nWTR [22]. In contrast, lower dose application dramatically decreased Hg-sorbed amount. Undoubtedly, increasing sorbent dosage will increase the ratio of nWTR to Hg ions causing more availability of adsorption sites since many authors found such observations [25,26]. The adsorbent dose of 0.10 g L^{-1} was used in the subsequent studies.

3.6. Sorption isotherms

Seven mathematical models were used to describe Hg sorption onto the three different particle sizes of WTR for reliable prediction of adsorption parameters including maximum sorption capacity. The parameters and the goodness of fit of the models used (Langmuir, Freundlich, Fowler–Guggenheim, Hill–de Boer, Temkin, Elovich, and Kiselev) [12,13] are presented in Table 1. The determination coefficients (R^2) of all the models tested were quite high especially for nWTR. The goodness-of-fit of the different 7 models tested shows that the Langmuir model yielded the lowest standard error (SE) values for all the sorbents studied followed by Temkin model (Table 1). The high SE values of Freundlich, Fowler–Guggenheim, Hill–de Boer, Elovich, and Kiselev models indicate the low predictive capability of these models to describe Hg sorption date (Table 1).

Table 1
Equilibrium model constants and standard error of estimate and determination coefficients for mercury adsorption by the three different particles sizes of WTR

Models	Parameter	mWTRs	μWTRs	nWTRs
Freundlich	K_F (mL g^{-1})	4.95	49.05	94.83
$q_e = K_F C_e^{1/n}$	$1/n$	1.30	0.96	3.08
	R^2	0.89	0.99	0.95
	SE	0.48	0.05	0.34
Langmuir	q_{max} (μg g^{-1})	3,900	7,000	50,000
$q_e = q_{max}\left(\frac{K_L C_e}{1} + K_L C_e\right)$	K_L (L mg^{-1})	3.333	200	250
	R^2	0.66	0.91	0.94
	SE	0.002	0.001	0.0001
Elovich	q_{max} (μg g^{-1})	1,428.57	5,000	20,000
$\frac{q_e}{q_m} = K_E C_e \exp\left(\frac{-q_e}{q_m}\right)$	K_E (L mg^{-1})	0.039	0.009	0.38
	R^2	0.73	0.88	0.90
	SE	0.43	0.07	0.22
Temkin	ΔQ (kJ mol^{-1})	20.71	14.56	3.04
$\theta = \frac{RT}{\Delta Q}\ln K_0 C_e$	K_0 (L mg^{-1})	11.980	4.96	3.21
	R^2	0.73	0.91	0.99
	SE	0.15	0.06	0.02
Fowler–Guggenheim (FG)	W (kJ mol^{-1})	2.001	1.13	3.35
$K_{FG} C_e = \frac{\theta}{1-\theta}\exp\left(2\theta\frac{w}{RT}\right)$	K_{FG} (L mg^{-1})	5.2320	21.28	87.73
	R^2	0.73	0.88	0.91
	SE	0.28	0.06	0.27
Kiselev	k_1 (L mg^{-1})	0.23	22.23	44.04
$k_1 C_e = \frac{\theta}{(1-\theta)(1+k_n\theta)}$	k_n	7.32	7.34	6.02
	R^2	0.66	0.91	0.94
	SE	2.62	156.09	265.9
Hill–deBoer	K_1 (L mg^{-1})	376.41	62.68	55.51
$K_1 C_e = \frac{\theta}{(1-\theta)}\exp\left(\frac{\theta}{(1-\theta)} - \frac{K_2\theta}{RT}\right)$	K_2 (kJ mol^{-1})	15.32	37.52	16.83
	R^2	0.98	0.93	0.99
	SE	0.22	0.19	0.19

q_e (mg g^{-1}) = Hg adsorbed per gram of adsorbent, C_e (mg L^{-1}) = equilibrium Hg concentration in solution, K_F = a constant related to adsorption capacity of the adsorbent (mg$^{1-(1/n)}$) $L^{1/n}$ g^{-1}), n = a constant, q_{max} (mg g^{-1}) is the maximum adsorption capacity of the adsorbent, K_L (L mg^{-1}) = Langmuir constant related to the free energy of adsorption, θ = fractional coverage, R = the universal gas constant (kJ mol^{-1} K^{-1}), T = the temperature (K), $\Delta Q = (-\Delta H)$ the variation of adsorption energy (kJ mol^{-1}), and K_0 = Temkin constant (L mg^{-1}), K_{FG} = Fowler–Guggenheim constant (L mg^{-1}), w = the interaction energy between adsorbed molecules (kJ mol^{-1}), k_1 = Kiselev constant (L mg^{-1}), k_n = a constant of complex formation between adsorbed molecules, K_1 = Hill–de Boer constant (L mg^{-1}), and K_2 (kJ mol^{-1}) = a constant related to the interaction between adsorbed molecules. A positive K_2 means attraction between adsorbed species and a negative value means repulsion.

3.7. Langmuir isotherm model

Mercury sorption conformed to the Langmuir model over the entire concentration range for all three particle sizes of WTR (Table 1 and Fig. 5(a)). The best fit of experimental data to Langmuir model suggested the homogeneous distribution of active sites on the adsorbent and monolayer mode of adsorption. The Langmuir maximum adsorption capacities (q_{max}) of mWTR, uWTR, and nWTR were calculated and found to be 3.9, 7.0, and 50 mg Hg g^{-1}, respectively (Table 1). The calculated q_{max} value of nWTR was 13 times higher than q_{max} of mWTR. The very high Hg sorption capacity (q_{max}) and Langmuir adsorption coefficient (K_L) values of nWTR in comparison with those of bulk WTR suggest that the nWTR is a superior sorbent for Hg.

3.8. Temkin isotherm model

Based on Temkin isotherm assumption, the sorption heat of adsorbate in a layer deceases linearly with surface coverage referring to the interaction between adsorbent and adsorbate [27]. The Hg sorption data onto the three particle sizes of WTR were analyzed according to the linear form of the Temkin isotherm, and the linear plots are shown in Fig. 5(b). The low SE values of Temkin model indicate that the model is successful in describing Hg sorption data on all three WTR particle sizes studied (Table 1). The negative values of adsorption energy, $\Delta Q = (-\Delta H)$, for all the studied WTRs, indicate the exothermic nature of adsorption reaction between WTR and Hg ions.

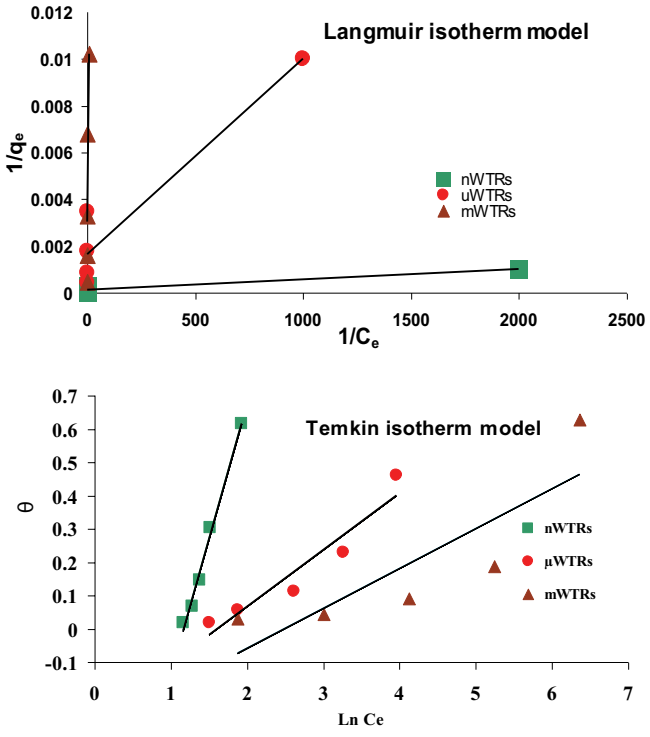

Fig. 5. Mercury sorption isotherm models: (a) Langmuir and (b) Temkin for different particle sizes of WTR.

3.9. Kinetics of Hg adsorption

The impact of contact time (15 min to 24 h) on Hg adsorption by nWTR at pH values 5, 7, and 9 was investigated, and the results are presented in Fig. 6. Adsorption of Hg by the nWTR increases rapidly during the first 15 min (Fig. 6) and then slows down considerably. Approximately 93% of Hg was adsorbed by nWTR within the first 15 min and slowly preceded to 98% sorption by the end of the 24 h period. Therefore, using nWTR in a single-step process (i.e. 15 min) for Hg removal is practical and highly efficient. The high accessibility of pore sites and the high tendency of Hg to bind with the functional groups may explain the rapid adsorption of Hg(II) ions by nWTRs in the initial fast adsorption step [28]. Similar biphasic Hg kinetic sorption data were reported for the Al_2O_3 [21]. The effect of solution pH on Hg adsorption by nWTRs is presented in Fig. 6. It was observed that Hg adsorption on nWTR declined as the pH increased from 5 to 9. Such decrease in Hg removal could be referred to the formation of weakly sorbed $Hg(OH)^{-3}$ complexes as a result of increasing OH^- ligand concentration with increasing pH. The high removal efficiency at low pH is attributed to the less competition from protons to reaction sites and to the increase in concentration of Hg^{2+} species which in turn favors formation of ≡M–OH–Hg bonds [26]. At high pH values, the predominant mercury oxyanion species such as $Hg(OH)_2$ compete with the highly negative surface hydroxide resulting in low mercury adsorption [26,29]. Similar results were reported by Barrow and Cox [30]. They reported that the maximum sorption of Hg(II) by geothite occurred at pH ~4 and decreased with further increase in pH.

The data of Hg adsorption kinetics at three pH solution values (5, 7, and 9) were fitted to four different kinetic models [31]. The higher R^2 and the much lower SE values of the power function models than those of parabolic, Elovich, and first-order models (Table 2) suggest that the predictive capability of the power function model to describe sorption data is quite high (Table 2 and Fig. 7). The adsorption kinetics of some heavy metals on Fe oxide adsorbent was also reported to follow power function model [22]. From Table 2, it can be shown that the adsorption rate (k_a) of the power function model decreased from 5.62×10^4 to 1.59×10^4 min^{-1} with the increase in the system pH from 5 to 9, indicating that Hg sorption is favored at low pH values.

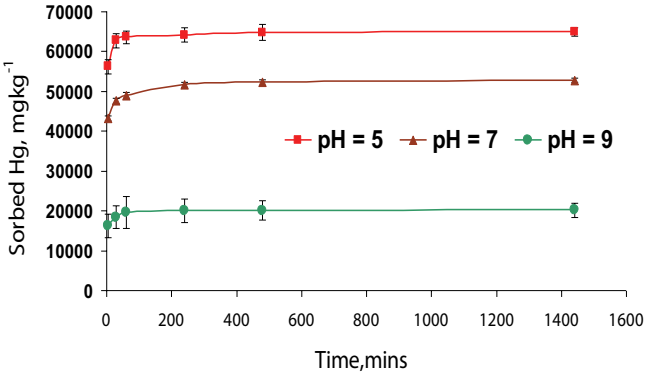

Fig. 6. Effect of contact time on the removal of Hg by nWTR at three different pH values.

Table 2
Kinetic model constants, determination coefficients, and standard error of estimate for mercury adsorption by nWTR at 3 pH values

Models	Parameter	pH_5	pH_7	pH_9
Elovich $q_t = \left(\frac{1}{\beta}\right)\ln(\alpha\beta) + \left(\frac{1}{\beta}\right)\ln t$	α (mg g^{-1} min^{-1})	3.02×10^{20}	4.69×10^{13}	4.86×10^{12}
	β (mg g^{-1})	7.10×10^{-4}	5.81×10^{-4}	1.43×10^{-3}
	R^2	0.76	0.95	0.84
	SE	0.18×10^{4}	0.92×10^{3}	0.69×10^{3}
First order $\ln(q_0 - q) = a - k_a t$	K_d min^{-1}	−0.007	−0.006	−0.007
	a (μg g^{-1})	8.24	8.76	7.58
	R^2	0.85	0.92	0.85
	SE	0.65	0.38	0.71
Parabolic diffusion $q = a + k_d t^{1/2}$	k_d (μg g^{-1} $min^{-1/2}$)	162.51	222.73	83.28
	a (μg g^{-1})	6.03×10^{4}	4.61×10^{4}	1.78×10^{4}
	R^2	0.42	0.67	0.50
	SE	0.28×10^{4}	0.23×10^{4}	0.12×10^{4}
Power function $q = k_a C_0 t^{1/m}$	k_a min^{-1}	5.62×10^{4}	4.17×10^{4}	1.59×10^{4}
	$1/m$	0.023	0.036	0.038
	R^2	0.75	0.94	0.83
	SE	0.013	0.009	0.017

q or q_t = Hg adsorbed (mg kg^{-1}) at time t, q_o = Hg adsorbed (mg kg^{-1}) at equilibrium, k_a = apparent sorption rate coefficient, α = the initial adsorption rate (mg g^{-1} min^{-1}), β = a constant related to the extent of surface coverage (mg g^{-1}), a = a constant; k_d = apparent diffusion rate coefficient, q = adsorbed Hg (mg kg^{-1}), C_o = initial As concentration (mg L^{-1}), t = reaction time (min), k_a = sorption rate coefficient (min^{-1}), and $1/m$ = constant. R^2 = determination coefficient, SE = standard error of estimate.

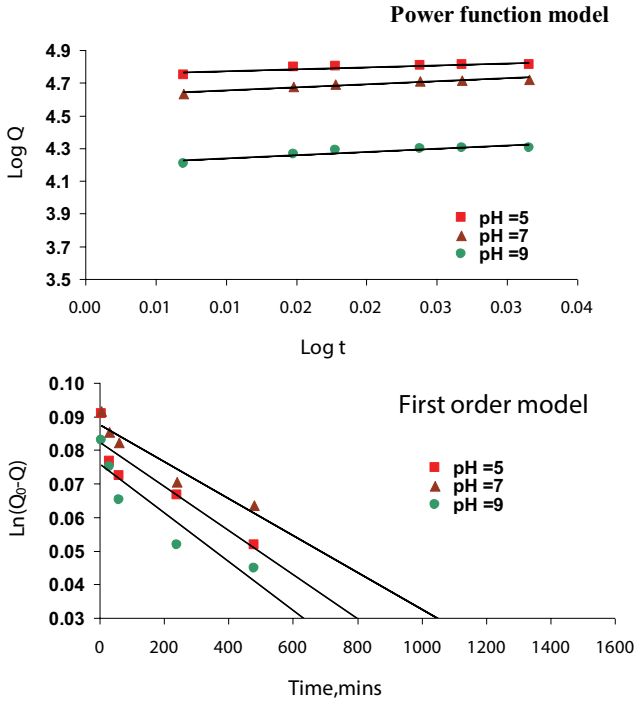

Fig. 7. Power function (a) and first-order kinetic plots (b) for Hg adsorption on nWTR at different pH values.

3.10. Selection of the operating conditions for Hg removal

3.10.1. Effect of initial solution pH on Hg removal

The effect of different pH values ranging from 3 to 11 on Hg adsorption onto nWTR is showed in Fig. 8. As seen, the adsorption reaction of Hg by nWTR was highly affected by pH variance since high amount of adsorbed Hg occurred at pH 3. Adsorption of Hg decreases rapidly with increasing pH until pH 11. The high Hg removal efficiency at pH 3 could be attributed to the fact that adsorption reaction of Hg onto oxide minerals favors at low pH and declines with increasing pH [29]. This finding demonstrates the ability of using nWTR to remove Hg in an acidic pH range.

3.10.2. Initial Hg concentration and competitive adsorption behavior

The effect of initial Hg concentration at the range of 5–160 mg L^{-1} on adsorption capacity of nWTR is illustrated in Fig. 9. It is apparent from the figure that increasing initial concentration resulted in noticeable increase in the quantity of Hg adsorbed. Initial metal concentration may encourage the adsorbate movement from the bulk solution to the adsorbent surface because the increase in the mass driving force arises from high initial concentration [32]. Furthermore, increasing initial adsorbate concentration enhances the interaction between adsorbent and adsorbate [33,34]. Fig. 10 also demonstrates the adsorbed amount of Hg in the presence or absence of competing cations such as Cr and As. The nWTR capability

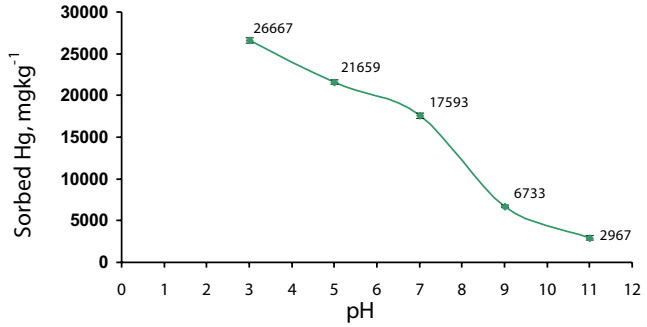

Fig. 8. Effect of pH on Hg adsorption by nWTR.

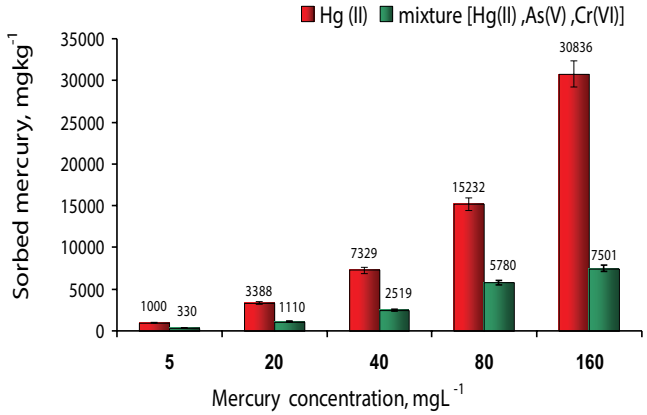

Fig. 9. Hg(II) adsorption in the presence of two competing ions at different initial Hg concentrations. Notice that the removal of Hg by nWTR was markedly affected by the presence of As (V) and Cr (VI).

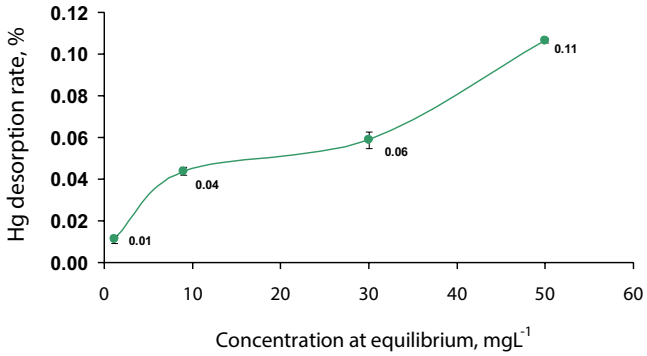

Fig. 10. Percentage of Hg desorbed from nWTR after four consecutive cycles.

for removing Hg was highly affected by the presence of As and Cr ions in solution. For instance, at high Hg initial concentration, Hg removal dramatically decreased from 96% to 23% due to competition between Hg and As/Cr cations for available sorption sites of nWTR. Similarly, Sun et al. [35] found an inhibition of Hg adsorption onto synthetic FeS due to the existence of Mn and Cu cations.

3.10.3. Desorption of Hg

The strength of Hg-loaded nWTR to resist four consecutive desorption cycles at different Hg concentrations from 5 to 500 mg L^{-1} (at pH 7.0) was studied to demonstrate the degree of Hg stabilization into nWTR. Weight of 0.1 g of Hg-loaded nWTR and 10 mL of high-purity water were mixed together in 50 mL capped polyethylene tubes, shaken for 24 h, and filtered. Following this, the filtrate was acidified and kept refrigerated for Hg determination. The percentage amounts of Hg desorbed after four consecutive cycles are illustrated in Fig. 10. As seen, there is a slight increase in Hg desorbed amounts from 0.01% to 0.11% due to Hg concentration increase. Obviously, the low percentage (0.11%) of Hg released after four consecutive cycles even at the highest Hg concentration load reflects an irreversible sorption reaction between Hg and nWTR and confirms the high stability of Hg into nWTR [23,36].

3.10.4. Repetitive application of nWTR

To assess the reusability of nWTR, series of experiments were performed in successive adsorption trials. A 0.1 g dose of nWTRs was placed in a 50.0 mL falcon tube, and aliquots (10.0 mL) of 10.0 or 100.0 mg L^{-1} Hg solutions were added and shaken for 30 min. After centrifugation, the solution was acidified and refrigerated for Hg analysis. The nWTR adsorbent which was left from the first adsorption trial was used for the next adsorption process. Such adsorption trial was repeated seven times for each nWTR sample and each Hg solution concentration used. The quantities of Hg sorbed in each successive adsorption trials are shown in Fig. 11(a). As shown, Hg(II) sorption decreased by 90% at the second adsorption trial for both initial Hg concentrations used and gradually diminished through the following adsorption trials. This could be explained on the bases that the most active sites of nWTR were occupied with the irreversible Hg during the previous adsorption step. Nevertheless, the cumulative Hg sorption during the seven successive adsorption trials for both initial Hg concentrations was increased by around 20% at the end of these trials (Fig. 11(b)).

3.10.5. Efficiency of Hg(II) removal from wastewater

The efficiency of nWTR for Hg removal was determined by conducting a batch experiment using industrial wastewater. Four samples were collected from wastewater discharged from food processing plant by using polyethylene bottles. The wastewater was characterized in terms of pH, electric conductivity (EC), Hg concentration, and major and minor elements. One liter of each water sample was spiked with 100 mg L^{-1} of Hg^{+2}, and 25 mL was placed in a 50 mL falcon tube along with 0.1 g nWTR. The mixture was shaken for 2 h and centrifuged at 4,000 rpm for 20 min, and the solutions were filtered and analyzed for Hg by ICPS. The pH and EC of the wastewater were 8.1 and (3.11 ± 0.11 dS m^{-1}), respectively. The predominant anions in the water were chloride (22.15 ± 1.65 mg L^{-1}), nitrate (18.09 ± 2.54 mg L^{-1}), and phosphate (6.55 ± 0.33 mg L^{-1}), and the sodium adsorption ratio was (6.12 ± 0.89). Amounts of Cu (0.09 ± 0.01 mg L^{-1}), Cd (0.04 ± 0.002 mg L^{-1}), Cr (0.40 ± 0.03), As (3.00 ± 0.09 mg L^{-1}),

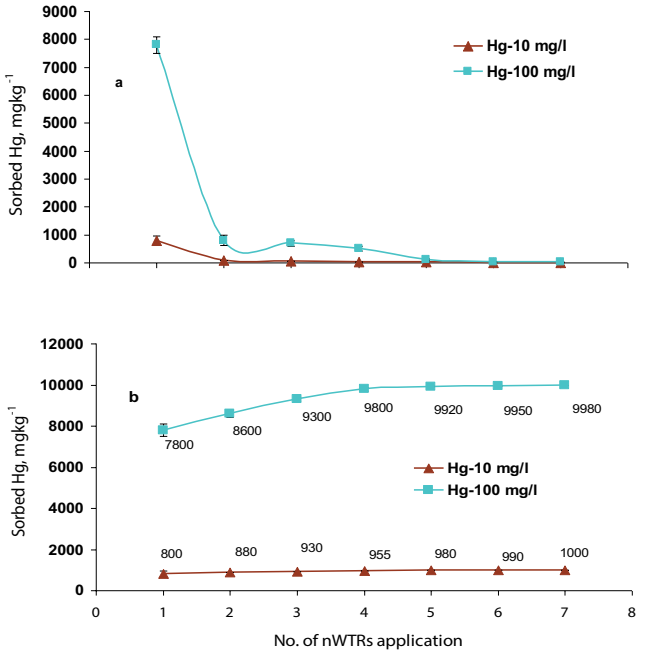

Fig. 11. The quantities of sorbed Hg in each successive adsorption trials (a) and the cumulative sorbed Hg during the seven successive adsorption trials. Initial Hg concentration in the solution was 10 or 100 mg L^{-1}.

and Pb (2.22 ± 0.05 mg L^{-1}) were also detected. The efficiency of nWTR for Hg removal from wastewater samples studied was 98.35%.

4. Conclusions

The potential of nWTR for Hg(II) removal from real wastewater was assessed using batch test. The nWTR sorbent showed fast and high efficient removal (98.35%) of Hg ions from contaminated industrial wastewater. According to Langmuir model, the calculated maximum sorption capacity (q_{max}) of nWTR for Hg(II) was 13 times higher than q_{max} of mWTR. The excellent performance of nWTR was mainly attributed to its high surface area and the presence of O–H and O–Al–O groups as active sites for Hg(II) sorption. In addition, the amount of Hg(II) released from Hg-loaded nWTR after four consecutive desorption cycles was very low (0.11%), which indicates the high stability of Hg sorbed by nWTR. Thus, the tested nWTR can be used as an efficient low-cost sorbent for Hg(II) removal from contaminated wastewater.

References

[1] P.K. Rai, Heavy metal pollution in aquatic ecosystems and its phytoremediation using wetland plants: an eco-sustainable approach, Int. J. Phytorem., 10 (2008) 131–158.
[2] G. Drasch, M. Horvat, M. Stoeppler, Mercury, E. Merian, M. Anke, M. Ihnat, M. Stoeppler, Eds., Elements and Their Compounds in the Environment: Occurrence, Analysis and Biological Relevance, Vol. 2, Wiley-VCH, Weinheim, 2004, pp. 931–1005.
[3] M. Yeganeh, M. Afyuni, H. Khoshgoftarmanesh, L. Khodakarami, M. Amini, A.R. Soffyanian, R. Schulin, Mapping of human health risks arising from soil nickel and mercury contamination, J. Hazard. Mater., 244 (2013) 225–239.
[4] C.G. Rocha, D.A.M. Zaia, R.V. da Silva Alfaya, A.A. da Silva Alfaya, Use of rice straw as biosorbent for removal of Cu(II), Zn(II), Cd(II) and Hg(II) ions in industrial effluents, J. Hazard. Mater., 166 (2009) 383–388.
[5] U.S. Environmental Protection Agency, Treatment Technologies for Mercury in Soil, Waste, and Water, Office of Superfund Remediation and Technology Innovation, Washington DC, 2007.
[6] N. Savage, M.S. Diallo, Nanomaterials and water purification: opportunities and challenges, J. Nanopart. Res., 7 (2005) 476–486.
[7] R.P. Schwazenbach, B.I. Escher, K. Fenner, T.B. Hofstetter, C.A. Johnson, U. von Gunten, B. Wehrli, The challenge of micropollutants in aquatic systems, Science, 313 (2006) 1072–1077.
[8] E.A. Elkhatib, A.M. Mahdy, M.N. ElManeah, Drinking water treatment residuals effects on nickel retention in soils: a macroscopic and thermodynamic study, J. Soils Sediments., 13 (2013) 94–105.
[9] E.A. Elkhatib, M.L. Moharem, Immobilization of copper, lead, and nickel in two arid soils amended with biosolids: effect of drinking water treatment residuals, J. Soils Sediments., 15 (2015) 1937–1946.
[10] A. Hovsepyan, J.J. Bonzongo, Aluminum drinking water treatment residuals (Al-WTRs) as sorbent for mercury: implications for soil remediation, J. Hazard. Mater., 164 (2009) 73–80.
[11] A.G. Caporale, P. Punamiya, M. Pigna, A. Violante, D. Sarkar, Effect of particle size of drinking-water treatment residuals on the sorption of arsenic in the presence of competing ions, J. Hazard. Mater., 260 (2013) 644–651.
[12] E.A. Elkhatib, A.M. Mahdy, K.A. Salama, Green synthesis of nanoparticles by milling residues of water treatment, Environ. Chem. Lett., 13 (2015) 333–339.
[13] E.A. Elkhatib, A.M. Mahdy, F.K. Sherif, K.A. Salama, Water treatment residual nanoparticles: a novel sorbent for enhanced phosphorus removal from aqueous medium, Curr. Nanosci., 11 (2015b) 655–668.
[14] J.A. Ippolito, K.A. Barbarick, H.A. Elliott, Drinking water treatment residuals: a review of recent uses, J. Environ. Qual., 40 (2011) 1–12.
[15] S. Brunauer, P.H. Emmett, E. Teller, Adsorption of gasses in multimolecular layers, J. Am. Chem. Soc., 60 (1938) 309–3019.
[16] Y. Zhang, M. Yang, X. Dou, H. He, D. Wang, Arsenate adsorption on an Fe-Ce bimetal oxide adsorbent: role of surface properties, Environ. Sci. Technol., 39 (2005) 7246–7253.
[17] D.A. Skoog, F.J. Holler, T.A. Nieman, Principles of Instrumental analysis, 5th Ed., Harcourt Brace and Co., Orland, 1998.
[18] V.M. Bermudez, Effect of humidity on the interaction of dimethyl methyl phosphonate (DMMP) vapor with SiO_2 and Al_2O_3 surfaces, studied using infrared attenuated total reflection spectroscopy, Langmuir, 26 (2010) 18144–18154.
[19] P. Tarte, Infra-red spectra of inorganic aluminates and characteristic vibrational frequencies of AlO_4 tetrahedra and AlO_6 octahedra, Spectrochim. Acta, 23 (1967) 2127–2143.
[20] J. Zou, Y. Dai, C. Tian, K. Pan, B. Jiang, L. Wang, W. Zhou, G. Tian, X. Wang, Z. Xing, H. Fu, Structure and properties of noncrystalline nano-$Al(OH)_3$ reclaimed from carbonized residual wastewater treatment sludge, Environ. Sci. Technol., 46 (2012) 4560–4566.
[21] A. Tessier, P.G.C. Campbell, M. Bisson, Sequential extraction procedure for the speciation of particulate trace metals, Anal. Chem., 51 (1979) 844–851.
[22] C. Kim, J. Rytuba, G. Brown, EXAFS study of mercury (II) sorption on Fe-and Al-(hydr)oxide: effects of pH, J. Colloid Interface Sci., 271 (2004) 1–15.
[23] K.D. Quinones, A. Hovsepyan, A. Oppong-Anane, J.C.J. Bonzongo, Insights into the mechanisms of mercury sorption onto aluminum based drinking water treatment residuals, J. Hazard. Mater., 307 (2016) 184–192.
[24] C.H. Giles, T.H. MacEwan, S.N. Nakhwa, D. Smith, Studies in sorption. Part XI. A system of classification of solution

adsorption isotherms, and its use in diagnosis on adsorption mechanisms and in measurement of specific surface areas of solids, J. Chem. Soc., 111 (1960) 3973–3993.
[25] M. Tanzifi, S.H. Hosseini, A.D. Kiadehi, M. Olazar, K. Karimipour, R. Rezaiemehr, I. Ali, Artificial neural network optimization for methyl orange adsorption onto polyaniline nano-adsorbent: kinetic, isotherm and thermodynamic studies, J. Mol. Liq., 244 (2017) 189–200.
[26] E. Elkhatib, A. Mahdy, F. Sherif, H. Hamadeen, Evaluation of novel water treatment residual nanoparticles as a sorbent for arsenic removal, J. Nanomaterials, Vol. 2015, Article ID 912942, pp. 1–10. DOI: 10.1155/2015/912942.
[27] M.J. Temkin, V. Pyzhev, Recent modifications to Langmuir isotherms, Acta Physiochim, URSS, 12 (1940) 217–222.
[28] J. Awing, X. Feng, C.W. Anderson, Y. Xing, L. Shang, Remediation of mercury contaminated sites - a review, J. Hazard. Mater., 221–222 (2012) 1–18.
[29] E.K. Faulconer, N. Hoogesteijn von Reitzenstein, D.W. Mazyck, Optimization of magnetic powdered activated carbon for aqueous Hg(II) removal and magnetic recovery, J. Hazard. Mater., 199–200 (2011) 9–14.
[30] N.J. Barrow, V.C. Cox, The effects of pH and chloride concentration on mercury sorption. 1. by goethite, J. Soil Sci., 43 (1992) 295–304.
[31] E.A. Elkhatib, J.L. Hern, Kinetics of phosphorus desorption from Appalachian soils, Soil Sci., 145 (1988) 11–19.
[32] K.P. Lisha, M.M. Shihabudheen, T. Pradeep, Manganese dioxide nanowhiskers: a potential adsorbent for the removal of Hg(II) from water, Chem. Eng. J., 160 (2010) 432–439.
[33] R. Saravanane, T. Sundararajan, S.S. Reddy, Efficiency of chemically modified low cost adsorbents for the removal of heavy metals from waste water: a comparative study, Indian J. Environ. Health, 44 (2002) 78–87.
[34] A.R. Kaveeshwar, S.K. Ponnusamy, E.D. Revellame, D.D. Gang, M.E. Zappi, R. Subramaniam, Pecan shell based activated carbon for removal of iron(II) from fracking wastewater: Adsorption kinetics, isotherm and thermodynamic studies, Process Saf. Environ., 114 (2018) 107–122.
[35] Y. Sun, D. Lv, J. Zhou, X. Zhou, Z. Lou, S.A. Baig, X. Xu, Adsorption of mercury (II) from aqueous solutions using FeS and pyrite: a comparative study, Chemosphere, 185 (2017) 452–461.
[36] E. Elkhatib, M. Moharem, A. Mahdy, M. Mesalem, Sorption, release and forms of mercury in contaminated soils stabilized with water treatment residual nanoparticles: effect of nanoparticles on mercury release and species in soils, Land Degrad. Dev., 28 (2017) 752–761.